2

Modelling Metallic Nanowires Breakage for Statistical Studies: Ni Case as Example

Samuel Peláez[1], Carlo Guerrero[2,3], Ricardo Paredes[2],
Pedro A. Serena[1], and Pedro García-Mochales[4]
[1]*ICMM, Consejo Superior de Investigaciones Científicas;*
[2]*Instituto Venezolano de Investigaciones Científicas;*
[3]*La Universidad del Zulia;*
[4]*Universidad Autónoma de Madrid*
[1,4]*Spain;*
[2,3]*Venezuela*

1. Introduction

During the last two decades, the study of the properties of nanowires has been one of the keystones for the development of nanotechnology since these nanometric size objects exhibit electrical and mechanical properties of interest in fundamental knowledge as well as for the future development of technological applications. In particular, many experimental studies have afforded the creation, stabilization and deformation of metallic nanowires in order to describe their mechanical properties and their electronic transport quantum features appearing due to electron transversal confinement (Serena & Garcia, 1997; Agraït et al., 2003). The standard approximation for the experimental study of such metallic nanowires includes the formation, elongation and breakage of ultranarrow nanocontacts, as for instance, those formed between an STM tip and a metallic surface. Since the atomic arrangement formed during every indentation-breakage cycle of the STM tip is different, these experimental studies require the accumulation and analysis of a huge amount of data to characterize the electron transport properties of the resulting nanocontacts.

With the advent of powerful computational resources and the achievement of realistic descriptions of the atomic interactions, it has been possible to reproduce "in silicon" many of such formation-breaking experiments. An important part of these simulation studies has been done using Molecular Dynamics (MD) algorithms, allowing to elucidate how this formation-elongation-breakage occurs. Furthermore, MD simulations allow the accurate determination of the different structures that appear during the final stages of the breaking process. Getting insight of such structures is a crucial matter since they control the electron transport through the nanowire, allowing a comparison with the experimental data.

However, the comparison between experimental results and MD computational simulations requires an extra ingredient: the use of statistics. In general, the study of nanoscale systems demands a statistical approach. This becomes more evident in electron transport studies, since little modifications of the atomic positions results in large conductance variations. It is

Source: Electrodeposited Nanowires and Their Applications, Book edited by: Nicoleta Lupu,
ISBN 978-953-7619-88-6, pp. 228, February 2010, INTECH, Croatia, downloaded from SCIYO.COM

necessary to statistically address the study of many nanowire breaking events, mimicking the experimental indentation-retraction cycles. In these cases, semiclassical approximations based in accurate interatomic potential are usually used since they are much less demanding of computational resources than sophisticated but time consuming *ab initio* methods.

MD simulations have not only proved successful in accounting for complex properties of many nanowires during the breaking process, allowing to detect the presence of ultranarrow structures as monomer, dimers and long atomic chains (Bahn & Jacobsen, 2001) that govern the electrical properties of the nanowire just before its breaking. MD techniques have also used to demonstrate the formation of new non-crystalline structures, as helical or weird structures (Gülseren et al., 1998), not corresponding to the initial FCC or BCC crystallographic disposition of the metal under study. This is also the case of the icosahedral or pentagonal nanowires formed by subsequent staggered parallel pentagonal rings (with a relative rotation of π/5) connected with single atoms (Mehrez & Ciraci, 1997; García-Mochales et al., 2008a; Peláez et al., 2009), showing a characteristic -5-1-5-1 ordering that have been confirmed experimentally for some metallic species (González et al., 2004).

In this chapter we will describe how to simulate the breakage of nanowires using MD techniques with Embedded Atom Method potentials, although the MD approach can be used with any other semiclassical potential (Section 2). We will describe the methodology used to extract different physical magnitudes of interest from the simulation, in particular the minimum cross-section that allows monitor the evolution of the breaking nanowire (Section 3). Also we shall describe the computational tools and algorithms applied to identify and characterize the different atomic structures formed that are relevant to the mechanical and transport properties of these nanocontacts: (i) monomers and dimers (and their surrounding environments) just before the breakage occurs (Section 4); and (ii) pentagonal nanowires formed during last stages of the elongation process (Section 5). We will show the procedure to calculate the atomic stress and apply it to investigate the pentagonal nanowires formed during the stretching process (Section 6).

Finally we will show how the statistical results corresponding to different stretching directions can be merged in order to compare with experimental findings (Section 7). This merging procedure is needed since experimental data usually correspond to the statistical average of nanowire breaking events involving random stretching directions. Although the method and a brief discussion will be given at Section 7, results expected for random stretching orientations will be included in its corresponding figures throughout the chapter for an easy comparison with those obtained for well determined stretching directions.

All these simulation and characterization methods will be focussed on the study of the breaking mechanisms of nickel nanowires, as a study case. The study will account for three stretching (crystallographic) directions, two initial sizes and a large range of temperatures. The statistical MD approach will describe hundreds of breaking events. The dependence of the breakage behaviour with several parameters (that can be controlled in experiments) will permit to determinate the optimal conditions for the production of some specific structures (monomer and dimer point-contacts, icosahedral nanowires) for this metallic species.

2. Computational methods

Our approach is based on the statistical study of the structural evolution of many nanowires under stretching, using standard Molecular Dynamics (MD) simulations. Each breakage

event, even starting from identical initial conditions, evolves showing its own features. Therefore, the only possibility to carry out an accurate study of the mechanical and electrical properties of the breakage process is performing a statistical analysis. We follow a similar strategy to the experimental one, simulating hundreds of independent breaking events, in order to determine the presence of preferred configurations. In particular, we have developed a methodology (Hasmy et al. 2001; Medina et al., 2003; Hasmy et al., 2005; García-Mochales et al., 2005) able to generate hundreds of computational breaking events and analyse them statistically to determine the different structures appearing at the breaking processes. We will describe this methodology along next sections.

In general, there are many computational simulations focused on the description of single nanowire breaking events, neglecting the study of statistical effects due to their high computational cost (Olesen et al., 1994; Bratkovsky et al., 1995; Barnett & Landman, 1997; Sørensen et al., 1998; Ikeda et al., 1999; Branício & Rino, 2000; Bahn and Jacobsen, 2001; Heemskerk et al., 2003; Sutrakar & Mahapatra, 2009), but several MD studies have statistically established that there exist a correlation between preferred atomic configurations and experimental conductance histograms at different temperatures (Hasmy et al. 2001; Medina et al., 2003; Hasmy et al., 2005; García-Mochales et al., 2005; Pauly et al., 2006; García-Mochales et al., 2008a; García-Mochales et al., 2008b).

Of course the price to pay for carrying out these statistical studies is the need to use "cheap" computational potentials for describing the atomic interactions. In spite of their accuracy, the large computational resources required by *ab initio* based methods make them inappropriate to determine computationally statistical features of these systems. A high computational effort is also required when other approaches are used, as tight-binding molecular dynamics simulations (González et al., 2004) or hybrid algorithms (Hasmy et al., 2005; Pauly et al., 2006). This means that semiclassical potentials, due to their relatively low resources requirements, are nowadays the most appropriate for statistical studies. On the other hand, "cheap" not mean "unaccurate", since we need to rely on obtained results of breaking nanowires. In consequence, the chosen potential must be complex enough to accurately reproduce low coordination situations as those appearing during the stretching process and structures with high surface/volume ratios.

We have simulated the nanowire atoms evolution using a MD scheme where atomic interaction is represented by Embedded Atom Method (EAM) potentials (Daw & Baskes, 1983; Foiles, 1985). On the EAM approach, the potential energy function for the system reads

$$E = \frac{1}{2}\sum_{ij}\varphi(r_{ij}) + \sum_{i} F(\bar{\rho}_i) \tag{1}$$

where i and j run over the number of atoms. In the first term, $\varphi(r_{ij})$ corresponds to a pair potential depending only on the distance r_{ij} between every pair of "different" atoms i and j. The second term is the so-called embedding energy, which depends on the mean electronic density $\bar{\rho}_i$ at atom i's location. This electron density is approximated in EAM as the sum of the contributions due to the surrounding atoms, $\bar{\rho}_i = \sum_{i\neq j}\rho(r_{ij})$. The embedding energy is calculated by evaluating and summing the embedding function $F(\rho)$ at each atom's position. Depending on the material and the specific physical properties to be studied, different pair potential $\varphi(r_{ij})$, embedding energy $F(\rho)$, and density $\rho(r_{ij})$ functions can be defined.

The computational technique here described is a general one and can be used with any other semiclassical potential. However, in order to reach accurate results, it is important that the

chosen one provides a good description of low dimensional situations (monomers, dimers, chains, open surfaces, edges, regions with vacancies, etc). We have used the EAM parameterization proposed by Mishin et al. (1999). This parameterization is a state-of-the-art potential able to describe high and low coordinated systems as those found during the last nanowire breaking stages. It has been constructed by fitting almost 30 different properties obtained from experimental measurements or accurate *ab initio* calculations: bulk properties as cohesive energy, lattice constants, elastic constants, phonon dispersion curves, vacancy formation and migration energies, surface energies, … This EAM potential has been used to describe $Ni_{x=1,150}$ clusters (Grigoryan & Springborg, 2003) showing a good agreement with *ab initio* calculations and experimental data. These small clusters contain configurations with very different coordination numbers (ranging from 1 to 12), therefore including the typical coordination numbers we have found during the nanowire breakage processes.

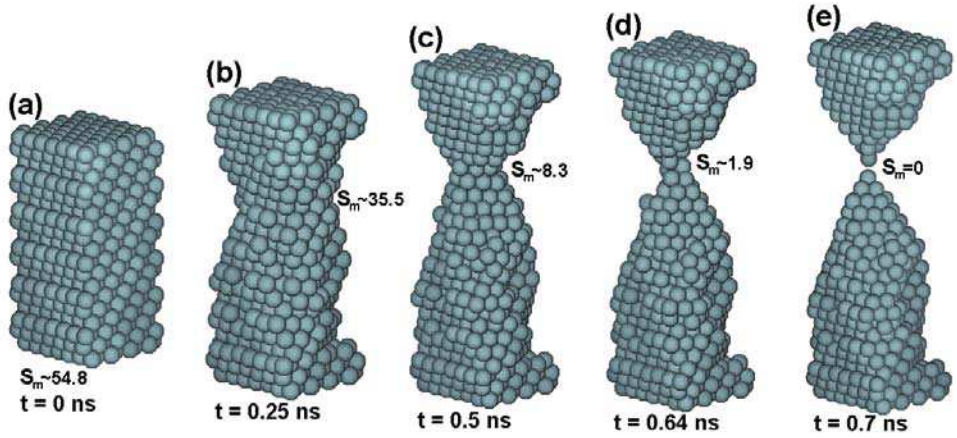

Fig. 1. Five different snapshots of a [111] Ni nanowire during stretching at T = 300 K from its initial parallelepiped shape. Each snapshot includes information on the simulation time and the minimum cross-section S_m at that time.

Nanowire dynamics has been studied at constant temperature T using a standard velocities scaling algorithm at every MD step (Rapaport, 1995). Nine temperatures ranging from 4 to 865 K (half of the Ni bulk melting temperature) have been considered in this work in order to describe the nanowire behaviour with the temperature. The time interval used for the integration of atomic trajectories (MD time step) is $\Delta t = 10^{-2}$ ps. Atomic trajectories and velocities were determined using conventional Verlet velocity integration algorithms. We have checked that results from this time step are equivalent to those obtained with shorter time intervals, ensuring the quality of the results with the smallest computational cost.

The simulation of a single nanowire breaking event consists of three stages. The first stage corresponds to the definition of the initial unrelaxed structure. We consider as initial nanowire a bulk super-cell with parallelepiped shape, containing hundreds of atoms ordered according to a FCC structure with bulk Ni lattice parameter (a = 3.52 Å). The initial parallelepiped height coincides with the stretching direction and is larger than the base edges. We define the z axis as the stretching (pulling) direction. In these studies we have considered three different stretching directions corresponding to the [100], [110] and [111] crystalline directions and two different parallelepiped sizes (large and small) with similar

aspect ratio for each direction. The initial sizes used were (layers × atoms per layer): for [100] case, 21×49=1029 atoms and 12×16=192 atoms; for the [110] case, 29×35=1015 atoms and 17×12=204 atoms; for the [111] case, 18×56=1008 atoms and 10×16=160 atoms. Fig. 1a shows the initial configuration corresponding to a large-type [111] nanowire. At the beginning of the simulation, each atom velocity is assigned at random according to the Maxwellian distribution corresponding to the simulation temperature (Rapaport, 1995).

The second stage corresponds to the relaxation of the bulk-like initial structure. Firstly, we define two supporting bilayers at the top and bottom of the supercell. Atomic x and y coordinates within these bilayers will be kept frozen during the simulation. The nanowire will remain attached to these two bulk-like supporting bilayers during the relaxation stage. This stage lasts for 3000 MD steps in order to optimize the geometry of the isolated parallelepiped-like nanowire. The role of these "frozen" bilayers is very important, since they represent the connection with the macroscopic world. If free or periodic boundary conditions were taken into consideration, the resulting nanowire evolution would present different patterns, including phase transformations upon loading as it has been noticed for narrow Ni nanowires (Liang & Zhou, 2006; 2007). During the third stage (stretching process), the z coordinate of those atoms forming the top (down) frozen bilayer is forced to increase (decrease) a quantity $\Delta z = 10^{-4}$ Å after every MD step. This incremental process simulates the separation of the supporting bilayers in opposite directions at constant velocity of 2 m/s, giving rise to the subsequent nanowire fracture. Those atoms located between the frozen regions move following the forces derived from their EAM-like interaction with the surrounding atoms. Notice that the stretching velocity is much larger than that used in experiments. However, our computational description of the nanowire breaking is comparable to that of actual experimental traces since the stretching velocity is smaller than the sound speed in nickel. We consider that the nanowire breaking process is completed when the minimum cross-section of the nanowire is zero (in the next section is explained the way this magnitude is calculated).

In Fig. 1 we depict five snapshots corresponding to different stages of a representative nanowire breaking process (a large nanowire stretched along the [111] orientation at 300K), starting with the initial (unrelaxed) configuration and finishing with the configuration just after the breakage. During stretching the nanowire shape develops through typical slip processes leading to inelastic deformations. Notice that during the last stages of the breaking process the nanowire structure evolves, forming a bipyramidal structure, each pyramid formed by three energetically favourable (111) facets.

3. Characterization of breaking nanowires: Cross-section histogram

During the stretching stage, the accurate knowledge of the atomic coordinates and velocities allows the full determination of the minimum cross-section S_m. This quantity provides relevant information on the favourable configurations appearing at the narrowest part of the nanowire during its evolution under stretching. Furthermore, S_m provides a first-order approximation of the conductance G (Sharvin, 1965). The minimum cross-section S_m is calculated in units of atoms following standard procedures that have been successfully used in previous studies (Bratkovsky et al., 1995; Sørensen et al., 1998). In our case, we define the atomic radius r_0 to be equal to half the FCC (111) interplanar distance ($r_0 = d_{111}/2$).

In order to calculate the cross-section S_i at a given z_i position, we firstly compute the total atomic volume $V_{\mathrm{tot},i}$ inside a "detecting cursor" width Δz. We have used $\Delta z = d_{111}$. We assign

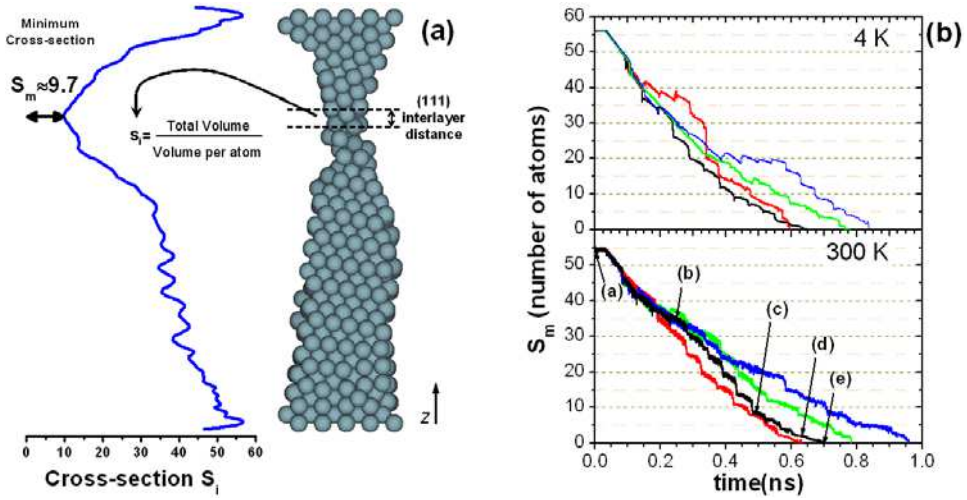

Fig. 2. (a) Example of how cross-section S_i is calculated along a [110] nanowire and its minimum value S_m (b) Evolution of the minimum cross-section S_m (measured in units of the number of atoms) as a function of time for four [111] Ni nanowires during their breaking process at two temperatures T = 4 K and T = 300 K. Labels (a)–(e) pointing at the black line correspond to the five different snapshots depicted in Fig 1.

a volume $V_0 = 4\pi r_0^3/3$ to each atom and, therefore, the quantity $S_i = V_{\mathrm{tot},i}/V_0$ corresponds to the nanowire section (in number of atoms) at the z_i position. In Fig. 2a is depicted a cartoon of the method used to measured S_i. The detecting cursor moves along the z axis between the two frozen bilayers, using a step equal to $0.1\times d_{111}$. This allows calculate the cross-section S_i along the nanowire. Finally, from the set of collected S_i values, we determine the minimum cross-section value S_m. Note that the cursor size Δz is kept fixed independently on the nanowire crystalline direction along the z axis. This allows a true comparison between histograms obtained for different orientations, especially at the last breaking stages. In our study S_m is calculated every 10 MD steps. In Fig. 2a we illustrate how the S_i and S_m are calculated with an example obtained from a [110] Ni nanowire simulation at 4K.

The evolution of S_m versus time shows a typical staircase trace. In Fig. 2b some examples of $S_m(t)$ illustrate this behaviour. $S_m(t)$ traces show a stepped profile with well-marked jumps associated to atomic rearrangements that take place within the nanowire. We have verified that these jumps are correlated with jumps in the force acting on the supporting slabs. In general, S_m decreases monotonically between two subsequent jumps reflecting the existence of elastic stages. These elastic stages have been associated to the experimentally observed conductance plateaus. As it is expected, the quantity S_m presents larger fluctuations when temperature increases, as it is shown when comparing the traces obtained at 4 and 300 K. These behaviours have been observed for the three stretching orientations.

Following the same methodology used in experiments, we summarize the information of many breaking events in histograms. In particular, the minimum cross-section histograms $H(S_m)$ are built by accumulating $S_m(t)$ traces acquired during the simulation of hundreds of nanowire stretching processes. We have show that 100 independent nanowire breakages can be enough to built a cross-section histogram, but more samples could be necessary for performing the statistical analysis of other quantities (García-Mochales et al., 2005).

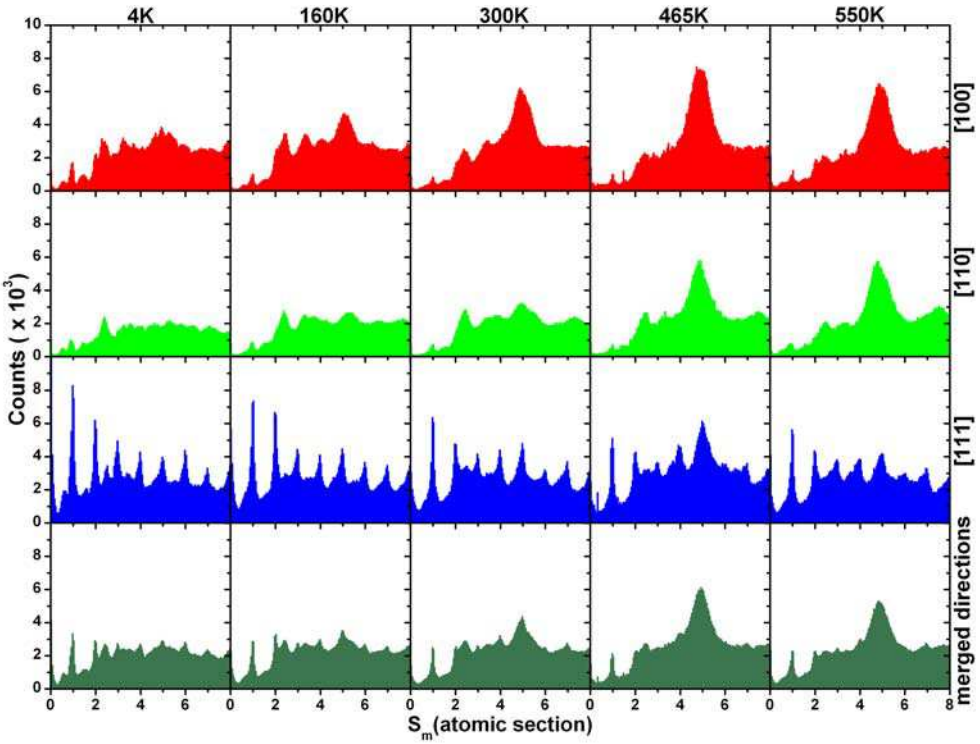

Fig. 3. Minimum cross-section histograms $H(S_m)$ of large Ni nanowires at T=4, 160, 300, 465 and 550K along the [100], [110] and [111] crystallographic directions. Last row show the expected results if nanowires would be stretched along random directions (see section 6).

In Figs. 3 and 4 (for large and small initial size nanowires, respectively) we show the histograms $H(S_m)$ for five temperatures (T=4, 160 300, 465 and 550 K), constructed with 300 independent breakages for the [100], [110] and [111] stretching directions. The different histograms are depicted in the range $0 < S_m < 8$. A first inspection of these figures reveals the existence of well-defined peaks associated to preferred nanowire configurations as it has been shown in previous works (Hasmy et al. 2001; Medina et al., 2003; Hasmy et al., 2005; García-Mochales et al., 2005).

Our main finding is that $H(S_m)$ histograms are very dependent on the stretching (i.e., the nanowire axis) direction. The $H(S_m)$ histograms associated to the [111] stretching direction present a well-defined peaked structure for both sizes at the whole range of temperatures depicted. The main difference we have found between both sizes corresponds to the small increase of the peak located at $S_m \sim 5$ above room temperature (RT) that only occurs for large size nanowires. For the [100] and [110] cases, very low temperature histograms present for both sizes a noisy structure. As temperature increases, histograms peaks show rounded shapes and the general structure presents less noise. The more prominent feature of [100] and [110] $H(S_m)$ histograms is the appearance and growth of a $S_m \sim 5$ peak as T increases (especially for small initial size nanowires). We will discuss later how this protruding peak, which is not developed at low temperatures and fade out at T > 650 K, is related with the

existence of (non-crystalline) icosahedral nanowires and it became the dominant structure at temperatures above RT. Apart the S_m ~ 5 peak, there are differences in the low S_m region between the [111] histograms and [100] and [110] ones. The [111] direction provides histograms with well-defined decreasing peaked structure whereas for [100] and [110] directions $H(S_m)$ presents a clear 'depletion' in the S_m < 2 region.

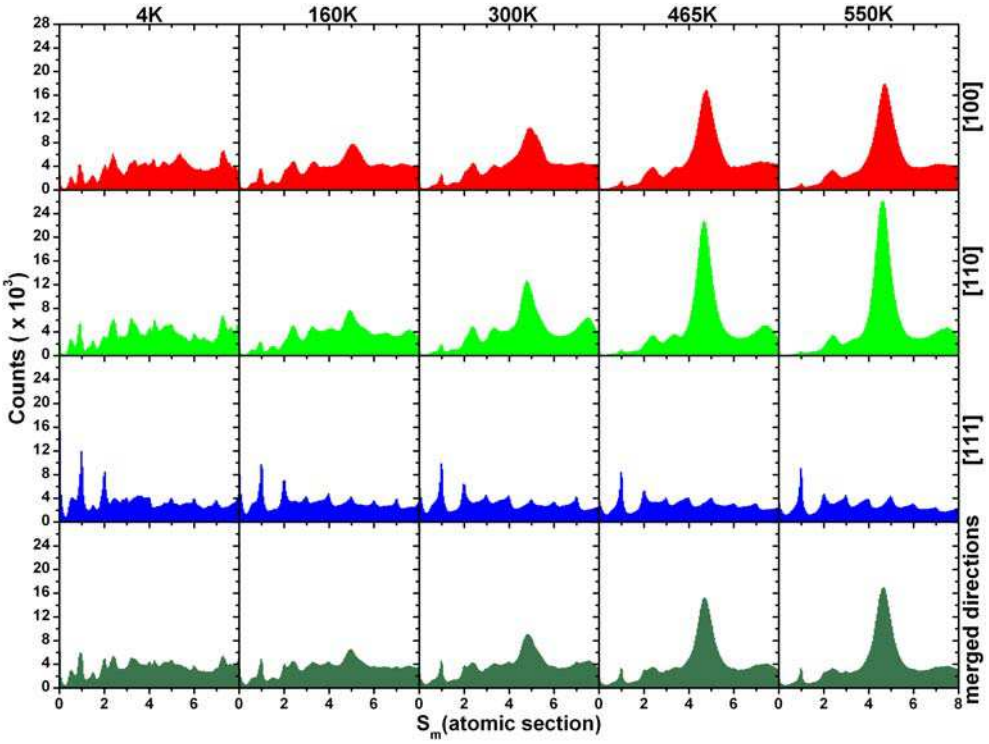

Fig. 4. Minimum cross-section histograms $H(S_m)$ of small Ni nanowires at T=4, 160, 300, 465 and 550K. Different rows correspond to nanowires stretched along [100], [110], [111] and random crystallographic directions.

The thermal evolution of histograms can be seen on the three nanowire orientations, but they are more remarkable for [100] and [110] stretching directions. Small peaks at T=4K correspond to metastable configurations with slightly higher cohesive energies with respect to other metastable configurations. The increase of temperature allows the exploration of more configurations during the stretching process, and, in this way, those metastable configurations with local minimum energy are easily accessible, leading to a better definition of their associated $H(S_m)$ peaks. For the three stretching directions, higher temperatures than those showed in Figs. 3 and 4 present a progressive vanishing of the peak structure. It is clear that at high temperatures the nanowire structures formation from stretching competes against nanowire melting processes (taking place at smaller temperatures than the bulk melting temperature). Nanowire atoms in a pre-melting state made progressively more difficult the formation of any stable structure.

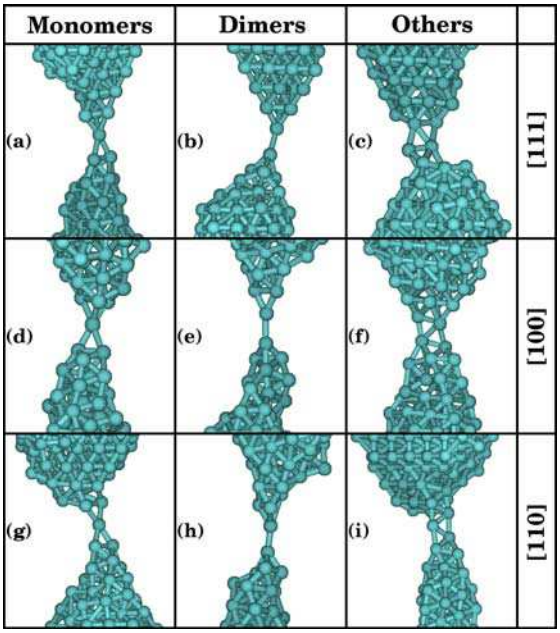

Fig. 5. Examples illustrating the type of nanowire configurations just before breakage at 4K. This classification scheme has been used for all the studied temperatures, since nanowire always break following these evolution patterns.

4. Characterisation of the nanowire before the breakage

4.1 Identification of monomers and dimers

Lowest conductance peaks observed in conductance histograms are associated with those configurations involving few atoms and appearing during the last breakage stages. We have found that final stages can be classified according to three different categories: monomers, dimers and "others" (as illustrated in Fig. 5). The monomer structure is characterized by a central atom standing between two "pyramids". In the dimer structure, the apex atoms of two opposite pyramidal configurations form a two atoms chain. Final configurations that do not match these two categories, presenting more complex structures, have been labelled as "others". As expected for Ni (Bahn & Jacobsen, 2001), we have not found any atomic chain formed by three or more atoms for the three studied stretching directions.

Complex structures (those labelled as "others") generally show an abrupt jump from $S_m \geq 2$ (i.e., structures formed by two or more atoms) to S_m=0. This feature could be used as a signature of such type of breaking pattern. On the other hand, monomers and dimers are characterized by similar S_m values (S_m~1), being difficult to distinguish among them if we only take into account the minimum cross-section value. We require an additional method to discriminate between monomer and dimer structures.

The procedure used is based on the "burning" algorithm introduced by Herrmann & Stanley (1984a; 1984b) to study the internal structure of percolating cluster at the percolation threshold. A simple generalization of this algorithm to disordered lattices was made to solve the problem that we are concerned. If an atom belonging to a monomer or dimer structure

is suppressed from the nanocontact, no connection will be between both sides of the wire. For this reason these objects (also called 'red' bonds) are the links in percolation theory. In a nanowire configuration, two atoms are identified as neighbours (i.e., they are linked) if its separation is smaller than a predefined distance d_{Cond}. This distance was chosen between the first and second nearest FCC neighbours distance.

The steps of the actual algorithm are: (i) Two atoms from both frozen sides of the wire are chosen. This atoms are called *a* and *b*. (ii) From atom *a* the structure is "burned" for the first time. This means that atom *a* is labelled *1*. All the neighbours of this atom are labelled *2*. Next, all the neighbours of atoms of type *2* are labelled *3* except atoms that were already labelled. This procedure is followed until the atom *b* is labelled as *n*. (iii) From atom *b* the structure is "burned" again. Atom *b* with label *n* and all its neighbours whose label is strictly lower than the label of atom *b* are separated in a new object. The neighbours with label *n*-2 from these atoms with labels *n*-1 are added to the new object, and so on. The procedure finish when atom *a* is added to the object. This object, called the elastic backbone, is the union of all the minimal paths between atoms *a* and *b*. It contains all atoms belonged to monomers and dimmers. (iv) To finally obtain monomers and dimmers, each atom for the elastic backbone is temporally separated from it and a burning procedure is running on this structure. This atom belongs to a monomer or a dimmer if no connection is observed. (v) In order to understand the structure of monomers and dimers, we also identify the neighbour atoms of those atoms forming the monomer or the dimer. To distinguish if they are connected to *a* or *b*, burning procedures are used.

We consider that two atoms are connected when the distance between their centres is lower than the distance d_{Cond}=3Å. Results using distances closer to the Ni nearest neighbours distance do not show relevant differences. Using this d_{Cond}, we have determined for each stretching nanowire the type of breaking pattern and analysed the statistical weights of monomers, dimers and complex structures appearing around the S_m~1 histogram peak for different simulation parameters (temperature, stretching direction, and initial size). In Fig. 6 the fractions of monomers, dimers and complex structures found in the range $0.25 < S_m < 1.75$ are depicted as function of the temperature for the two initial sizes of Ni nanowires.

These figures denote that the temperature have little influence on the production ratio of final structures. The main change is a slight decrease of other structures fraction with the temperature, especially for large size nanowires. Therefore, the decrease of S_m≈1 and S_m≈0.5 peaks with the temperature must be attributed to a decrease of the mean lifetime due to instabilities of these structures at high temperatures. This lifetime shortening is more remarkable for the dimer structure.

For the [111] stretching direction the joined proportion of monomer and dimers (~80%) is larger than the fraction of other structures (~20%). This fraction seems to be rather independent of the temperature as well as the nanowire size, except for small ones near the nanowire melting temperature, where monomers fraction increases and dimers fraction decreases. For the [100] and [110] cases, there is a large fraction of complex structures (30-40%). The temperature behaviour of this fraction shows a dependence on the nanowire size: it keeps constant for small size nanowires but decreases for the large size ones. The fraction of monomers is of the same order but slightly lower than that found for the [111] case, meanwhile the dimers fraction takes values below of the [111] case. On the contrary of the [111] case, dimers fraction increases with temperature for the large size nanowires set, especially if the stretching occurs along the [110] direction.

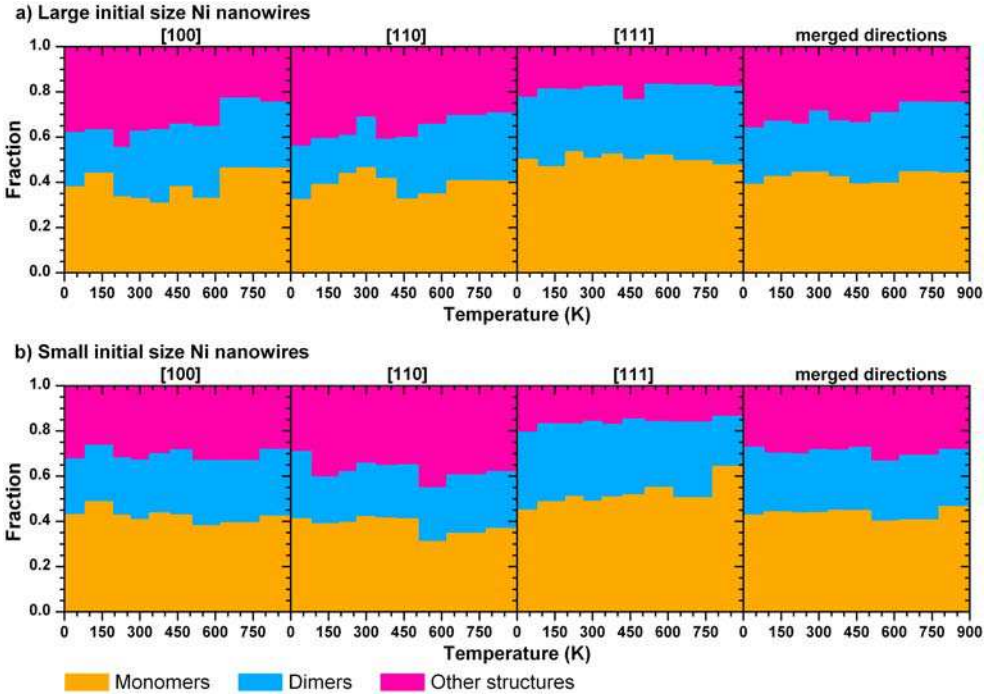

Fig. 6. Fraction of monomers, dimers and more complex structures appearing during the Ni nanowire breaking process as functions of the temperature for Ni nanowires of large (a) and small (b) initial size. Different columns correspond to nanowires stretched along [100], [110], [111] and random (merged) crystallographic directions.

Also the final structures of the nanowire at the breaking moment can be related with its whole evolution and the full histogram $H(S_m)$ building partial histogram that only include traces that present monomer and dimer configurations (García-Mochales et al., 2008). For the [111] stretching direction, that monomer and dimer based partial histogram is similar to the full histogram, indicating that the nanowire generally evolves from its initial structure to a monomer and/or dimer configuration before the breakage. This breaking scheme seems to be independent on the initial nanowire size and temperature. However, the behaviour of partial histogram for the [100] and [110] stretching directions depend on the initial nanowire size and temperature. For small nanowires with [100] and [110] orientation and at low temperatures the breaking pattern obtained for the [111] case is recovered: most of the nanowires present monomer or dimer configurations during the last stages of the elongation process and full and partial histograms are quite similar. As the temperature increases (and the S_m~5 peak appears) the histograms start to differ although the general shape is conserved. Nanowires forming monomers and dimers are responsible of the $0.25 < S_m < 1.75$ $H(S_m)$ region, but for larger sections they show a significantly lower contribution. For the largest nanowire case for [100] and [110] orientations, independently of the temperature, nanowires with monomer and dimer structures at the final breaking stage are solely responsible of those smaller peaks at the low S_m region, but do not recover the full peaked

structure appearing in $H(S_m)$. These divergences of the partial histogram from the full histogram (at high temperature for small nanowires, at any temperature for the large one) indicates that a relatively large proportion of nanowires do not break forming monomers nor dimers, being larger their number as the difference grows. Therefore most of the [100] and [110] large nanowires do not break forming monomers and dimers as final structure.

4.2 Local and non-local environment of monomer and dimer breaking configurations

Electron transport through a given breaking nanowire mainly depends on the size of the narrowest nanocontact cross-section. However, the atomic structure of neighbouring regions also plays a key role in the electronic conductance (Pauly et al., 2006; Hasmy et al., 2005). The study of the electronic transport through monomer-like or dimer-like Ni nanocontact has centred on static structures with surrounding configurations obtained from crystalline structures (Sirvent et al., 1996; Jacob et al., 2005), proposing 3-1-3 and 4-1-4 as the most likely monomer configurations. However, a visual inspection of monomers and dimers from our MD simulations confirms that their environment does not follow such crystalline-like pattern. The MD calculations allow us the accurate determination of the actual type of neighbourhood formed around monomers and dimers and their relative probability of appearance. In addition, this information could provide an estimation of the probability of conductance associated to the lower peaks of the S_m histograms.

The electron transport through the nanowire also depends on more factors, including the presence of disorder (defects, vacancies, impurities, dislocations …) along the nanowire. Its effect on the electrical conductance can be very important at the latest stages of the breaking process: if the scattering due to the disorder becomes very large, the electron transport could leave the ballistic regime and quantum diffusive transport features should appear.

Once the atom that forms the monomer is identify, it is trivial to determine its neighbour atoms (those closer than the distance d_{Cond}) and classify them with respect to the monomer z coordinate. This gives us a configuration of type "n-1-m", i.e., a configuration where there are n atoms at one side of the monomer and m atoms at the other side. For dimer structures the procedure is similar, providing configurations of type "n-1-1-m".

In Fig. 7 we present the occurrence probability of different atomic configurations around monomers and dimers, showing that the atomic structures (and its probability of occurrence) around monomers and dimers are roughly the same regardless of the size of the initial nanowire, the stretching direction or the temperature (although only T=4 and 300K are showed). We notice that the most likely monomer structure presents the configuration 2-1-3. Around 40% of the monomers exhibit this configuration. Besides, we found that 2-1-4, 3-1-3, 3-1-4 and 2-1-2 configurations appear with a probability ranging between ~20% and ~10%. Some small deviations from this rule can be found for the [110] and small size nanowires: at low temperature 2-1-2 configuration presents a probability larger than 30% but 3-1-3 structure have less than a 5%, whereas at RT probability of the 3-1-3 configuration is higher than the 20% (growing at the expense of the 2-1-3 structure). Comparing the actual monomer surrounding structures with those proposed on previous works, the non-trivial 2-1-3 structure (the most probable, as we found) was not even considered. Moreover, we have not found evidences of the 4-1-4 crystalline-like configuration in our simulations.

In Figs. 7 the local environment for the dimer configurations show that the most common structures are 3-1-1-4, 3-1-1-3 with occurrence probability between ~50% and ~20%. The most likely configuration depends slightly on the temperature, size and stretching direction of the nanowire. The 4-1-1-4 configuration has also a relative high probability (~10%-20%),

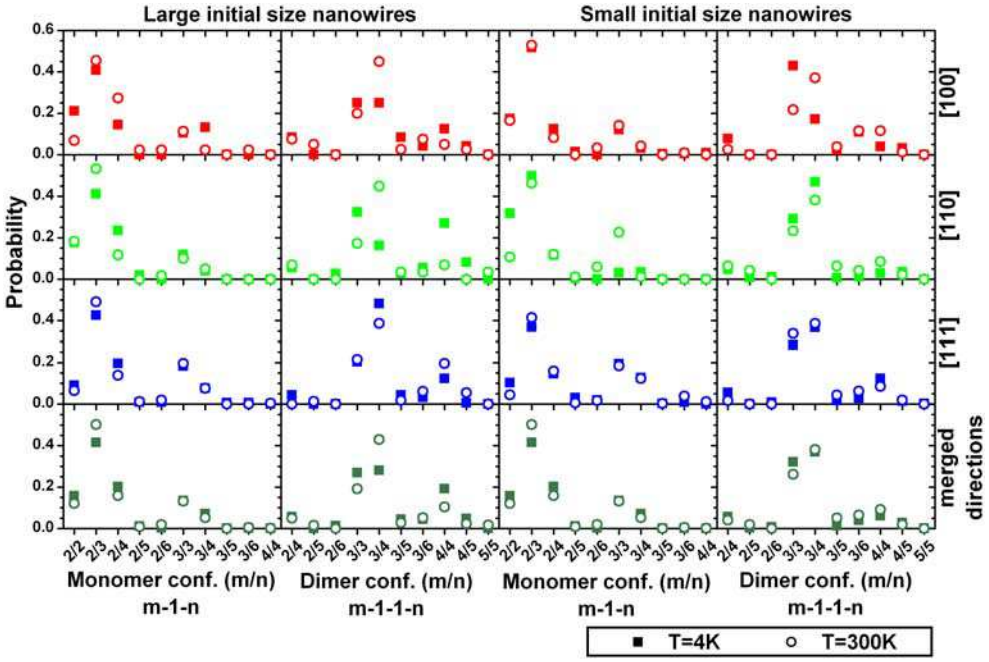

Fig. 7. Probability of the occurrence of different atomic environments around a Ni monomer and a Ni dimer for different stretching directions and temperature T=4 and 300K. A "m/n" configuration means that the monomer (dimer) configuration is of the type "*m*-1-*n*" or "*n*-1-*m*" (type "*m*-1-1-*n*" or "*n*-1-1-*m*").

being for the [110] stretching direction, low temperature and large initial size nanowire more probable (~30%) than the 3-1-1-4 configuration (that decreases below 20%). Other configurations show probabilities lower than 5%, reflecting that each dimer atom has to be connected with a stable base formed by 3 or 4 atoms.

As previously mentioned, the electron transport through the nanowire is also dependent on the existence of disorder along the nanowire. To determine the existence of a long-range structure (order) on the monomer configuration at T=4K, in Fig. 8 we plot the average number of atoms $\langle N(z)\rangle$ located at a distance z from its position. This approximation will detect if the atomic structure keeps its crystalline character as the z distance from the monomer (or dimer) increases. We have calculated $\langle N(z)\rangle$ for the three stretching directions and two initial sizes. There is not significant difference between the two sizes, both show similar $\langle N(z)\rangle$ values up to 8 Å and the decrease observed from this distance for smaller nanowires is expected due to their size. A similar behaviour is observed around dimers (not shown).

On one hand, for the [111] case, we note clear peaks separated a distance close to the typical separation of the [111] planes d_{111}=2.03Å, indicating that the system try to keep the same crystallographic structure from both fixed slabs towards the monomer position. On the other hand, for the [100] and [110] stretching directions, the situation is quite different, since for increasing z we could not distinguish a well defined peaked structure. For these orientations, the fixed slabs try to maintain the [100] or [110] structure but nanowires present dislocations, disorder and the formation of large non-crystalline areas leading to

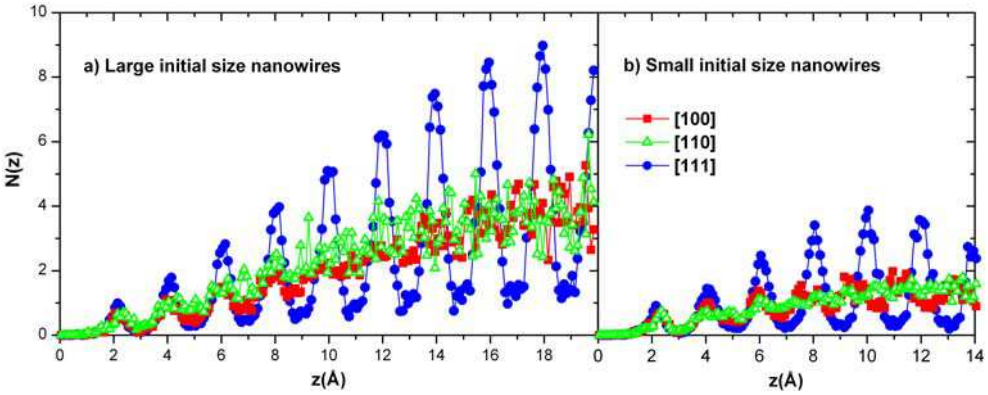

Fig. 8. Average number of atoms $\langle N(z)\rangle$ at a distance z from the monomer position for the [100], [110] and [111 directions at T=4K: large (a) and small (b) initial size nanowires.

amorphization of the nanowire. Similar behaviour has been previously noticed for infinite nanowires under high strain rates (Branicio & Rino, 1999; Ikeda et al., 1999).
As pointed previously, the amorphization of the structure can be important in the electronic transport during latest stages of the nanowire breakage: the presence of disorder on a large nanowire region will lead to a conductance decrease. But in this case is especially important because we could observe two transport behaviours depending on the stretching direction. In the [111] case the electron moves inside a well ordered system (keeping the ballistic transport features), meanwhile for the [100] and [110] orientations the electron suffers many scattering events due to the disorder (leading to a diffusive transport regime).

5. Icosahedral or Pentagonal nanowires: Identification and characterisation

In previous subsections we showed that $H(S_m)$ presents a huge peak around S_m~5 for the [100] and [110] cases and that the peak increases with the temperature. We have analyzed the types of configurations which contribute to this peak. We have depicted in Fig. 9 different time snapshots of one of those structures, for a [110] nanowire at T=550K, showing its formation, growth and breakage. It presents along its length pentagonal rings (responsible for the S_m~5 cross-section value) that name these structures: pentagonal nanowires. We found that these structures (for the Ni case) are very common for the [100] and [110] stretching directions, whereas they rarely occur for the [111] case.
Icosahedral or pentagonal nanowires are formed by subsequent staggered parallel pentagonal rings (with a relative rotation of $\pi/5$) connected with single atoms, showing a characteristic -5-1-5-1- ordering (see as example Fig. 9). The atomic sequence -5-1-5-1- presents a fivefold symmetry with respect to the nanowire axis. This symmetry does not correspond to any crystallographic FCC nor BCC structures. The -5-1-5-1- staggered nanowire configuration may be understood in terms of a sequence of interpenetrated icosahedra. This icosahedral symmetry is very common in very small systems due to the large stability and high coordination characterizing such geometry (Bulienkov & Tytik, 2001). Contrary to monoatomic chains, pentagonal nanowires are rather robust structures at relatively high temperatures and, therefore, they may consider as a promising candidate for being used as nanodevice components.

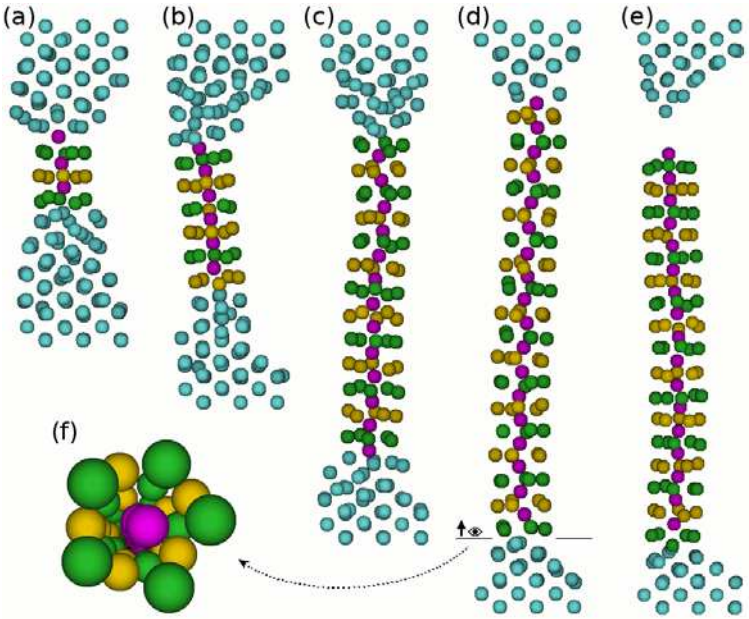

Fig. 9. (a-e) Formation, growth and breakage of an icosahedral nanowire from a small [110] Ni nanowire at T=550K; (f) shows the cross-sectional perspective view as seen from the position indicate on (d). Colours are used to identified the -5-1-5-1- structure.

Different computational works during the last decade have shown the formation of these structures on different metallic species. The formation of staggered pentagonal configurations during the stretching process has been already reported for Na (Barnet & Landman, 1997) using first principles methods, and for Cu nanowires with different Molecular Dynamic (MD) approaches (Mehrez & Ciraci, 1997; Gülseren et al., 1998; González et al., 2004; Sutrakar & Mahapatra, 2009). In particular the high stability of the Cu nanowire was confirmed with ab-initio calculations. Pentagonal motives also appear in infinite Al and Pb nanowires obtained from MD simulated annealing methods (Sen et al., 2002). More recently we have reported such structures for stretched Ni nanowires with different crystallographic orientations (Garcia-Mochales et al, 2008a; 2008b; 2008c), being very stable and presenting a high plastic deformation under strain.

The formation of pentagonal nanowires can be seen in the curve S_m vs. time as a plateau around S_m~5. Its large statistical occurrence is reflected in histograms of minimum cross-section $H(S_m)$ as a huge peak centred at S_m~5. These quantities (the length of those cross-section plateaus, the relative height or area of that peak) were proposed as parameters to classify the conditions and probability of formation of the icosahedral nanowires. But these magnitudes provide little information about the actual lengths and the length distribution of such pentagonal chains and cannot determine either the number of pentagonal rings that form the tubular structure. To overcome these limitations, we developed an algorithm that identifies the pentagonal structures that form the icosahedral nanowire (Pelaez et al., 2009). This algorithm also allows us to define its length L_p as the distance between the outermost pentagonal rings and to count the number of pentagonal rings n_p that form it.

The algorithm is based in the determination of the angular distribution of the nearest neighbour atoms and provides a parameter ($\alpha(z)$) which compares the angular distribution of the projected nanowire atomic coordinates with that corresponding to a perfect pentagonal nanowire. For a given z coordinate we consider a slice perpendicular to the z (stretching) direction with a thickness of 2 Å and centred on the z value. The N_t atoms inside such slice are projected onto the xy plane, each one getting new 2D coordinate $\vec{\eta}_i$; then the centroid of this structure is calculated $\vec{\eta}_0 = \sum_i \vec{\eta}_i / N_t$. The angular distribution is calculated from the angles $\theta_{i,j}$ between the pairs of vectors $\vec{\eta}_i'$ and $\vec{\eta}_j'$ defining the projected atomic coordinates with respect to the centroid ($\vec{\eta}_i' = \vec{\eta}_i - \vec{\eta}_0$). The parameter α is calculated as

$$\alpha = \frac{2}{N_a} \sum_{i,j}^{N_a} \frac{|\theta_{i,j} - m\,\theta_0|}{\theta_0} \tag{2}$$

where N_a is the number of pair of atoms considered, θ_0=π/5 is the reference angle of a perfect staggered pentagonal structure and m is the integer that minimizes the expression $|\theta_{i,j} - m\,\theta_0|$. To avoid spurious contributions from atoms near the centroid, only vectors satisfying $|\vec{\eta}_j'| > a/4$ are considered, i.e., centre atoms are excluded from the calculation of α. This algorithm is applied along the z-coordinate of the nanowire, displacing the imaginary slab δz=0.1 Å at a time. This results in a $\alpha(z)$ profile of the nanowire, showing where pentagonal structures appear.

In order to minimize artifacts, the $\alpha(z)$ curve is softened over a Δz interval. This softened curve $\langle\alpha\rangle(z)$ is defined as

$$\langle\alpha\rangle(z) = \frac{1}{\Delta z} \int_{z-\Delta z/2}^{z+\Delta z/2} \alpha(z')\,dz' \tag{3}$$

where a value of Δz=1Å has been found appropriate. This average of α ($\langle\alpha\rangle$) over a 1Å interval provides a quantity that distinguishes between pentagonal and non-pentagonal structures through the nanowire. We have observed that if the parameter $\langle\alpha\rangle(z) < 0.5$, the set of atoms around z forms a structure similar to that of a pentagonal ring. On the contrary, if $\langle\alpha\rangle(z) > 0.5$ the set of atoms presents another structure (bulk like -FCC-, helical or disordered).

The ability of the algorithm to discriminate between different structures was checked using different test structures (square, pentagonal, hexagonal and heptagonal nanowires) with increasing amount of disorder (Peláez et al., 2009).

In order to further check the ability of the algorithm to identify pentagonal regions, we tested its performance over simulated nanowires showing icosahedral structure. Fig. 9 shows several snapshots of a nanowire breaking process where an icosahedral structure is observed. For these snapshots, Fig. 10 shows the $\langle\alpha\rangle(z)$ profile curves, as well as the radial and angular distribution functions $g(r)$ and $g(\theta)$ through different sections of the nanowire at snapshot (b). As illustrated in the figure, the algorithm returns value near to 1 when is applied to the ordered regions of the nanowire, and values below 1 for the pentagonal region. Minima of $\langle\alpha\rangle$ correspond to the position of the pentagonal rings; as they are not perfect ordered structures (though still can be recognized as pentagons) their $\langle\alpha\rangle$ values are a bit greater than zero. We have chosen the value of $\langle\alpha\rangle$=0.5 as the limit value to recognize a

pentagonal structure. This value ‹α›=0.5 discriminates between pentagonal and non-pentagonal structures. We define the pentagonal nanotube length $L_p(t)$, observed during stretching at a given time t, as the distance between the maximum and minimum z coordinates with ‹α›=0.5. We also define n_p as the number of pentagonal rings forming the icosahedral nanowire at its late stage (equivalent to the number of ‹α› minima below 0.5).

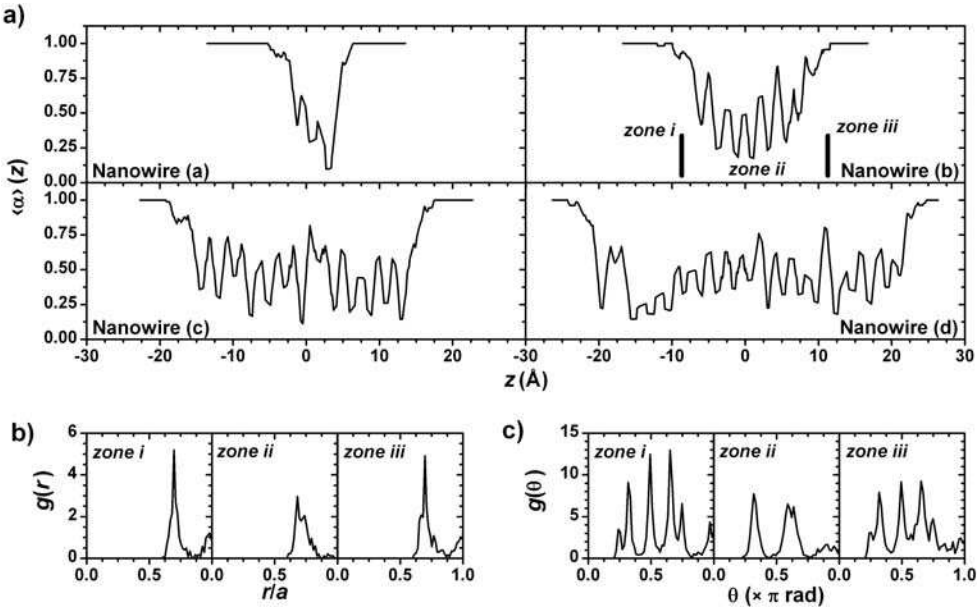

Fig. 10. a) Average α-parameter ‹α›(z) along the Ni [110] simulated nanowire showed in Fig. 9 before breakage. Minimum values of ‹α› below 0.5 correspond to the position of pentagonal rings forming the icosahedral nanowire. b-c) Distance $g(r)$ and radial $g(\theta)$ distributions for the three marked region of the nanowire labelled as (b).

In Fig. 10 we have also divided the nanowire in three regions that seem to have different structures from visual inspection. For each one of these three regions we show the radial and angular distribution functions $g(r)$ and $g(\theta)$. We can see that the outermost regions exhibit a mostly FCC structure, with the FCC typical interatomic distances and angles. The central region corresponds to the pentagonal structure according to both visual inspection and the ‹α› profile. Inspecting the angular distribution function in this region we can see how the central peak of the FCC structure has disappeared and the peak at the right has displaced a bit towards the left. This is the typical structure of the pentagonal angular distribution function. Regarding the interatomic distances, not a big change is appreciated in this region from the radial distribution function. As it can be seen, the parameter ‹α› proves to be a very efficient parameter to identify the pentagonal regions in a breaking nanowire.

We use this algorithm as the standard tool to characterize the pentagonal nanowires produced during the stretching simulations and extract information about probabilities of formation of such structures, distributions of their maximum lengths L_p^m (the length L_p of icosahedral nanowire just before its breakage) and the number of pentagonal rings n_p on the nanotube just before breaking. Since our simulation were carry out over a broad range of

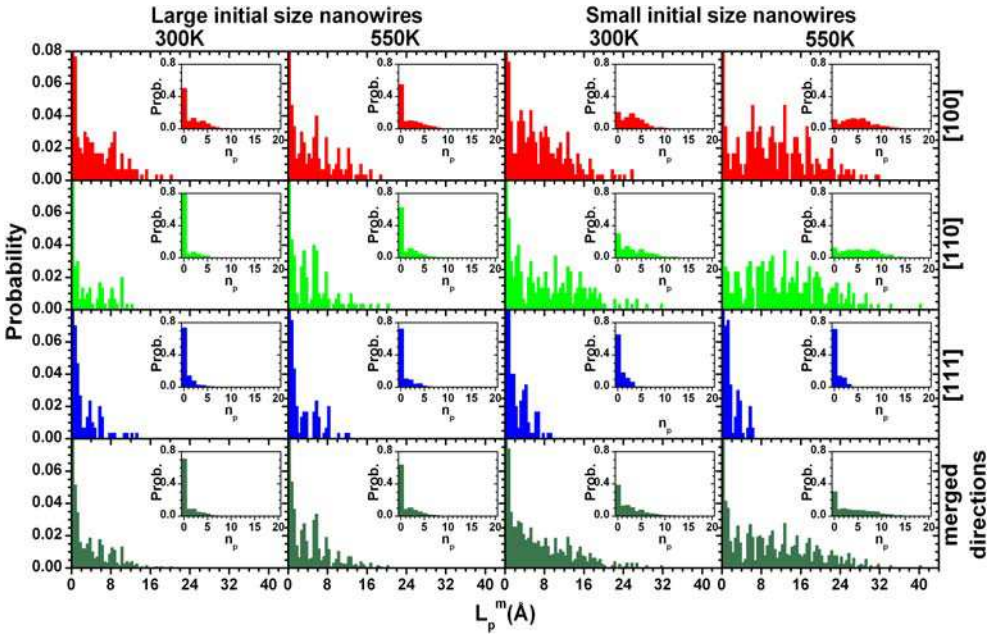

Fig. 11. Distribution function $D(L_p^m)$ for the maximum pentagonal nanowire length L_p^m and (as insets) distribution function $D(n_p)$ for the maximum number of pentagonal rings n_p for the two initial size nanowires at T=300 and 550K for [100], [110], [111] and random stretching directions.

temperatures, this studies will give the optimal temperature T_{Opt} required for maximizing the occurrence probability and/or length distribution of pentagonal nanowires.

In Fig. 11, for the three orientations and two sizes of nanowire considered, we have plotted the probability distribution $D(L_p^m)$ of obtaining a pentagonal nanowire of maximum length L_p^m. Also it is depicted, as insets, the probability distributions $D(n_p)$ of the maximum number of pentagonal rings. We only show results for two temperatures (T=300 and 550K). Distributions of L_p^m present a clearly peaked shape. It indicates that pentagonal chains have well defined favourable lengths. The peaks are separated approximately by integer values of the distance $d_{5\text{-}5}$=2.22 Å, the calculated equilibrium separation between successive staggered pentagonal rings (García-Mochales et al, 2008b; 2008c).

The distribution value for L_p^m=0 corresponds to those cases where the nanowire does not form any pentagonal structure (n_p=0). Those cases with 0 < L_p^m < 2 Å correspond to nanowires showing a unique pentagonal ring (n_p=1). We have considered that an icosahedral wire is formed only if the chain satisfies $n_p \geq 2$. The shortest pentagonal chain (n_p=2) presents a unique icosahedron in its structure. The L_p^m distributions of T=300 and 550K shown on Fig. 11 exhibit large tails corresponding to those pentagonal nanowires including a large number of pentagonal rings. Distributions from low temperatures (not presented here) show also a peaked structure, but they have a shorter tail and larger probability on the L_p^m < 2 Å region (Peláez et al., 2009). The same behaviour is observed for very high temperatures (as it approximates to the nanowire melting temperature).

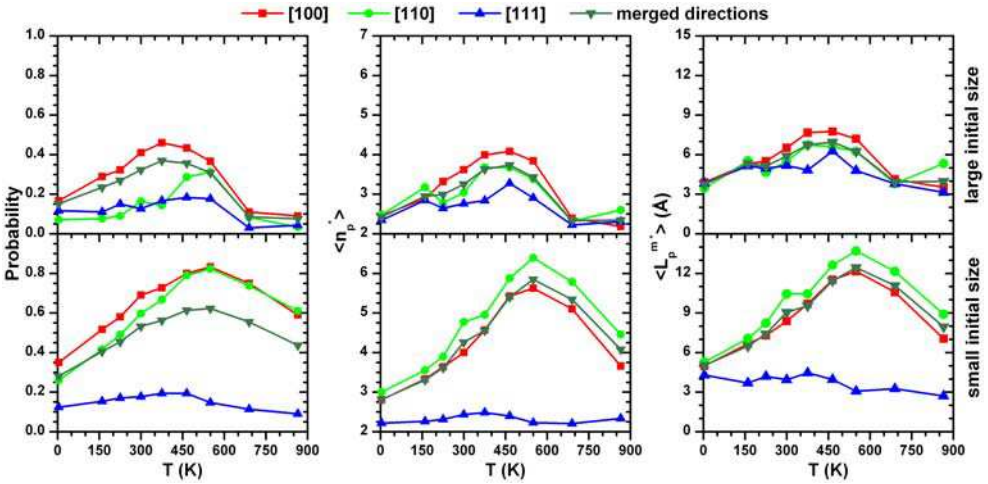

Fig. 12. Temperature dependence for the two initial sizes of the probability p_i of finding pentagonal chains (with number of pentagonal rings $n_p \geq 2$) and mean number of pentagonal rings $\langle n_p^* \rangle$ and mean length $\langle L_p^{m*} \rangle$ of such icosahedra chains detected.

$D(n_p)$ distributions are shown in Fig.11 for the same simulations sets. Usually $D(n_p)$ presents two maxima. The first one at n_p=0 identifies the breakages that do not produce icosahedral chains. It is the most probable case at all temperatures. The second maximum in a zone with $n_p > 2$ indicates that, once a seed is produced to nucleate a pentagonal wire, it will grow with high probability. This two-peak feature of the distribution occurs at any temperature except at very low or high temperatures. The position of the second maximum depends on breakage simulation set parameters (temperature, size, orientation), but it is correlated with the probability of formation of an icosahedral nanowire. And, as it is expected, the length of the $D(n_p)$ tail goes along with the $D(L_p^m)$ tail. Ideally every structure with $n_p \geq 2$ would give a sharp peak in the $D(L_p^m)$ distribution. Since real structures show tilted pentagonal rings, there is not perfect alignment with z-axis and the pentagonal rings separation is longer than that of the equilibrium, producing broad peaks in the $D(L_p^m)$ figure.

$D(n_p)$ determines the pentagonal wires production efficiency using the percentage p_i of breakages that produce an icosahedral chain, i.e, $p_i = \sum_{p \geq 2} D(n_p)$, elucidating which conditions favour the appearance of icosahedral nanowires. This is shown in left panels of Fig. 12 as function of the temperature for the three stretching directions and the two sizes. For same temperature and stretching orientation, it is easier to form a pentagonal tube if we start with a small size nanowire. The probability of getting icosahedral chains is much lower when breaking along the [111] direction than from the [100] or [110] directions. For the [111] breaking orientation this probability is below the 20% of the simulations, while for the other orientations the probability can be even over 80% for the small initial size nanowires.

In central and right panels of Fig. 12 are represented respectively the average number of pentagonal rings $\langle n_p^* \rangle$ and the average icosahedral tube length $\langle L_p^{m*} \rangle$ of those simulations that present a pentagonal nanowire during their stretching (i.e., the average is performed only over simulations with $n_p \geq 2$). Again the [111] orientation produces pentagonal nanowires of average length lower that those produced on the [100] and [110] orientation.

But in this case there are differences between the two initial nanowire sizes. For the small size, in average, the [111] orientation produces pentagonal tubes of bit more than 2 pentagonal ring while the other orientations produce much longer nanowires. For large size nanowires, average lengths of all orientations are more similar: $\langle n_p^* \rangle$ and $\langle L_p^{m*} \rangle$ of the [111] orientation grows with respect of the small size, and concurrently these quantities for the [100] and [110] directions decreases. Combining the information of these lengths with the information of the probability p_i, it can be seen that for small size nanowires it is highly probable to form an icosahedral nanowire for the [100] and [110] orientation and it would have a relative large length. For large nanowires these orientation would produce pentagonal nanowires at a quite good ratio, but their average size will be smaller. For the [111] orientation, both sizes would produce pentagonal chains at a low proportion, but if a large size initial nanowire is used, the length of the few created chains should be comparable with those produced from the [100] and [110] orientations.

Finally, from curves depicted in Fig. 12 we can extract information about the optimal temperature of creation of icosahedral nanowires. Maxima of these quantities indicate the optimal temperatures T_{Opt}. For each simulation set parameters (size and orientation) there can be two possible values of T_{Opt} depending on whether we are looking for the maximum probability of nanowire formation or the highest length of the pentagonal tube. Although slightly differences on the simulation parameters and the chosen criterion, T_{Opt} is around 550 K for parameters investigated. As it can be seen in Fig. 11, in this T_{Opt} temperature $D(L_p^m)$ and $D(n_p)$ show also the broadest distributions.

6. Atomic stress calculations

One of the advantages of the MD methodology is the possibility of analyzing mechanical properties of the systems. I.e., we are able to monitor the time evolution of the tensile atomic stress along the stretching direction of the nanowires. This measurement gives us information about the stress distribution on the nanowire at every stage of the breaking process. Fig. 13 shows an example of the time evolution of the atomic stress. When a

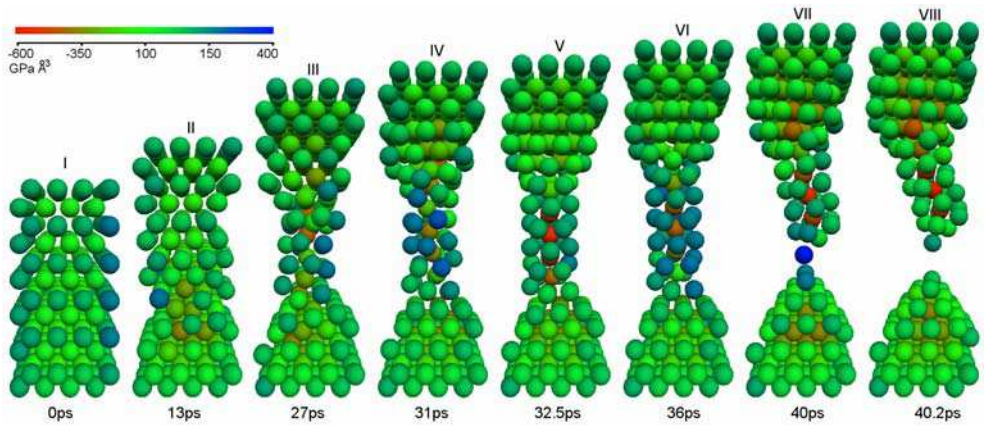

Fig. 13. Snapshots of the breaking process of a Ni nanowire that forms a pentagonal structure. Colours account for the atomic tensile stress.

simulation starts, the nanowire shape is that of a parallelepiped (snapshot I of Fig. 13). In these conditions those atoms at the edges of the structure are in a more stressed situation than those on the surfaces. And these atoms on the surfaces are more stressed than bulk ones. This stress distribution is related to the atomic coordination. Atoms at low coordination situations feel more stressed and unstable, while high coordination atoms are in a more comfortable condition.

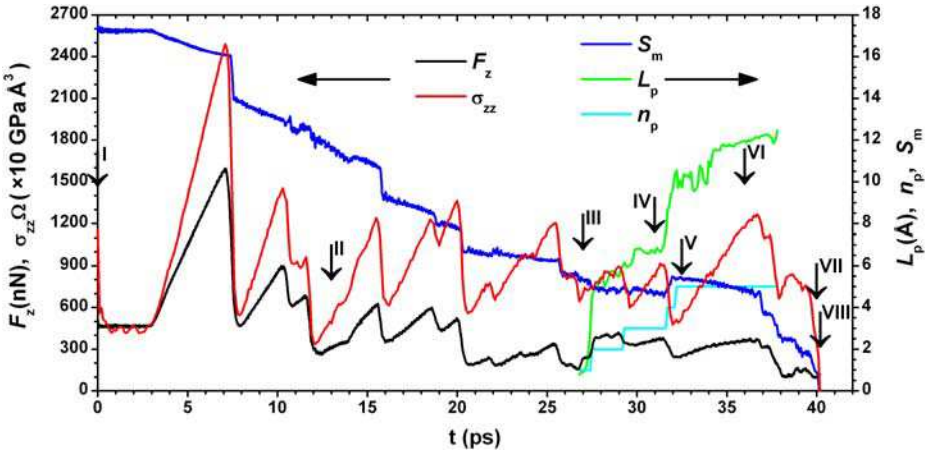

Fig. 14. Time evolution of several quantities from the simulation shown in Fig. 13: force F_z on the extremes of the nanowire; atomic stress σ_{zz} is shown here multiplied by the system volume Ω (constant during the simulation); minimum cross-section S_m; the pentagonal length $L_p(t)$ and the number of pentagonal rings $n_p(t)$ that form the pentagonal structure starting at $t \sim 26$ns. Vertical arrows indicate the time position of snapshots shown in Fig. 13.

It is well known that icosahedral is one of the preferred structures for small clusters and icosahedral arrangements are quite robust (Bulienkov & Tytik, 2001). However, the stability of pentagonal nanowires has not been studied so far. There is a large difference in the atomic coordination between those atoms in the core of the pentagonal nanowire and those on the surface. So we are interested in analyzing how the stress is distributed along this icosahedral configuration (within and around the pentagonal structure) during its formation, growth and breakage as the stretching process occurs.

As it can be seen in Fig. 13, an interesting behaviour of the atomic tensile stress is observed in the narrowest region of the nanowire (the central region) as the stretching process goes on. Since snapshot III, a clear distinction can be made between surface and core atoms. Atoms in the surface are much more stressed than core atoms. This means that surface atoms fell strained (they are bluer), while core atoms feel compressed (they are redder) compared to those atoms (green) out of the pentagonal structure. This can be understood the following way: the system tends to keep a uniform overall stress along all the regions of the nanowire. In the central region this means that the sum of the surface and core atoms tensile stress (weighted by the number of atoms of each kind) should be approximately equal to the overall average tensile stress of the nanowire. In this central region most of the atoms are on the surface. Having so few core atoms makes in compensation their compressive stress much stronger than the strained stress of surface atoms.

The uniaxial tensile stress σ_{zz} of the nanowire showed on Fig. 13 is depicted in Fig. 14. It is calculated from the virial theorem for static systems using the formula (Tsai, 1979)

$$\sigma_{zz} = \frac{1}{2V} \sum_{i,j} F_{ij} \frac{(r_{iz} - r_{jz})^2}{r_{ij}} \tag{4}$$

where V is the whole volume of the nanowire, $F_{i,j}$ is the force exerted by atom j over atom i, r_{ij} is the distance between them and r_{iz} is the z-coordinate of atom i.

Fig. 14 shows the time evolution of $\sigma_{zz}(t)$ and the force $F_z(t)$ on the frozen slabs of the nanowire. Both curves exhibit a sawtooth structure, with a similar behaviour. A linear increase with time is associated to an elastic strain, while an abrupt drop is related to plastic atomic rearrangements to release the elastic energy. Some of these F_z or stress drops coincide with a drop in the minimum cross section S_m, also shown in Fig. 14. In these cases the atomic rearrangements have driven the system to have a thinner cross section in its narrowest region. Notice, nonetheless, the particular case of the abrupt increase of S_m between snapshots IV and V. Fig. 13 shows that at snapshot IV the section where the central region and the bottom reservoir join is formed by a thin 4-atom structure. At snapshot V, however, this region has a more robust pentagonal structure that increases the cross section and relaxes the tensile stress.

Starting from snapshot III, our algorithm for detection of pentagonal structures shows the presence of pentagonal rings. In Fig. 14 we also plot the length of this pentagonal structure and the number of pentagonal rings detected. We can see that the path from having 2 to 3 pentagonal rings is accompanied by a drop in the tensile stress and the force F_z. Similar drops in S_m and F_z are observed when the system changes from 3 to 5 pentagonal rings. The variable L_p, also plotted in Fig. 14, illustrates how the pentagonal region elongates until a plastic rearrangement takes place and a new pentagonal ring is formed.

7. Comparing with experimental results

In previous sections of this chapter we have showed how, using powerful computational resources and accurate description of the atomic interactions, it is possible to reproduce many of the formation-breaking experiments "in silicon". And indeed, that it is possible to analyse situations and structures that experimentally are difficult to study. We have stressed the importance of statistical studies of these phenomena because, given a particular initial geometrical configuration and temperature, each breakage event evolves differently. Of course this is the standard approximation for the experimental study of metallic nanowires, where statistical data is accumulated during many indentation-retraction cycles.

However, the comparison between experimental results and the numerical simulations (as they have been presented up to here) requires an additional element. Experimental data usually correspond to the statistical average of nanowire breaking events involving random stretching directions. In a standard experiment there is no reason that indicates that any particular orientation would be preferred during the nanowire formation and breakage. Therefore, to accomplish a complete statistical analysis equivalent to the experimental one, computational calculations must simulate breaking events on random stretching directions. This could be a potential problem since it is not easy to perform simulations with arbitrary (random) initial stretching directions. Fortunately, it is not necessary to compute "every" stretching orientation to get the statistical behaviour of the breaking nanowires.

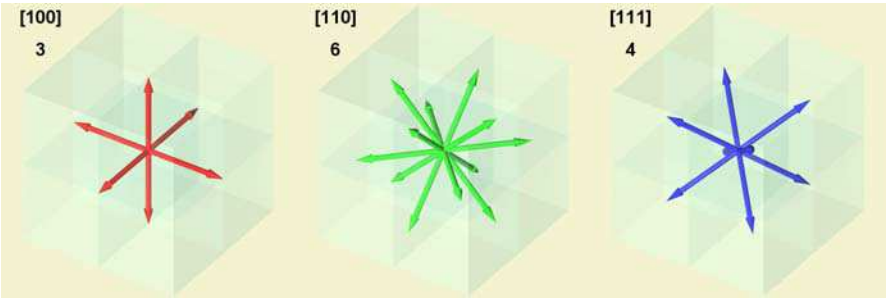

Fig. 15. FCC main crystalline directions ([100], [110], [111]) and their multiplicities (3, 6 and 4 respectively).

In an experiment, the final stages and behaviour of a nanowire during its breakage are leaded by the type of crystalline structure closest to its elongation direction. So it should be in simulations. Therefore, we need only to analyse main crystalline orientations, those that show different structural type, and average their results according to their occurrences. I.e., to achieve orientation statistics in computational simulations, results from the main crystalline directions have to be merged with the appropriate weights. These weights will be proportional to the zone axis multiplicity (González et al., 2004). Of course, each main direction must have an accurate statistics to guarantee the correctness of the global results.
Nickel has a FCC crystalline structure. In Fig. 15 we show FCC main crystalline directions ([100], [110] and [111]) and their multiplicities (3, 6 and 4 respectively). Their relative occurrence at random stretching orientation should be 3/13, 6/13 and 4/13. These are the weights we have used to merge the statistical results from the three main directions and obtain the average statistical results that can be compared with the experimental ones.
In figures showed in previous sections we have included these results corresponding to this weighted average. In Figs. 2 and 3, expected minimum cross-sections histograms for random stretching orientation are shown for large and small nanowires. Merged histograms conserve main features of [111] direction (well defined peaks for low S_m values) and [100] and [110] directions (huge peak at S_m~5 that increases with the temperature).
The merged results for the monomer and dimer production are shown in Fig. 6. For small sizes the proportion of monomer (~45%), dimers (~25%) and more complex structures (~30%) is constant with the temperature; for large systems, monomer ratio keeps constant (~45%) but that of dimers increases (~25 to ~30%) slightly with temperature. Their surrounding structures (Fig. 7, bottom panels) show the main characteristics already described. For monomer, the 2-1-3 structure is the most probable (~50%) followed by 2-1-4, 2-1-2, 3-1-3 and 3-1-4, independently of the temperature. No signal found from a 4-1-4 structure. For the dimer structure, the 3-1-1-4 configuration is the most probable one followed by the 3-1-1-3 and 4-1-1-4; their relative probabilities depend on the nanowire size and the temperature. With respect the non local environment, two different behaviours (that will be mixed in standard experiments) are expected if stretching occurs along the [111] direction (ordered structure from the monomer/dimer) or along the [100] and [110] orientations (amorphization around the monomer/dimer). This can lead to a mix of two transport regimes (ballistic and diffusive) in experiments were the conductance is measured.
The pentagonal nanowires production for the [100] and [110] directions is much higher than for the [111]. When results from the three directions are merged (Fig. 12), probabilities of

production of icosahedral chains are still quite high (~60% at the T_{Opt} for small size nanowires; ~30% for large ones) as well as their average length and number of pentagonal rings. Experiments between T=450 and 650 K will likely obtain icosahedral nanowires; even at RT it is relatively probable to produce such structures, although shorter ones.
Summarizing and putting into relation all this results, for conductance experiments of breakage of nanowires without orientation control, it is expected to observe quantum transport features at $S_m \leq 1$ associate with monomer and dimers and a characteristic signal associated with pentagonal nanowires (S_m~5). System just before breakage will show ballistic or diffusive electron transport characteristics depending on the random direction, producing probably broad and not well defined peaks at low values of the conductance histogram. To identify the formation of icosahedral nanowires, they should produce a broad peak at relative high conductance value, easily seen at temperatures above RT.

8. Conclusions and future work

In this chapter we have described the huge potential and reliability of MD techniques within the EAM framework as a tool for the description of the mechanical properties and atomic configurations of metallic nanowires. In particular, we apply this methodology to the study of nanowires subjected to a tensile stress leading to fracture, and studied the final stages of the breaking events when the nanowire narrowest region is formed by low coordination configurations. This computational approach goes beyond the description of isolated single breaking events and it is able to provide a statistical view of a large set of breaking events, mimicking the methods established in the laboratories long time ago.
We have presented several techniques to analyse the average behaviour of different physical magnitudes of interest provide by the simulation, as the minimum cross-section, the tensile stress, the local and non-local geometry of formed monomers, dimers and pentagonal chains. In particular we have introduced a procedure to merge results obtained from simulations with well defined stretching direction in order to reproduce more realistic experimental conditions where geometry of stretched nanowire is not so well defined.
The statistical approach and the analysis techniques has been used to compute and analyse hundreds of breaking events of Ni nanowires taking into account several parameters as the nanowire size, temperature, and crystallographic stretching direction. Results cover by this large set of variables would help to the interpretation of the experimental findings.
This powerful tool provides a new approach to understand many physical problems related with the behaviour of metallic nanowires. In particular, future work will address the study of formation of monomer, dimer, monoatomic chain and icosahedral structures for different metallic species. However, more open questions must be addressed, as the role of the initial nanowire shape and size especially if the initial cross-section shape corresponds to a magic number configuration. Or the responsibility of indentation-retraction processes in the formation of histograms: histograms presented in this chapter are formed by adding independent breaking events whereas in the experimental situation is slightly different, since all the contacts are formed in the same region. The technique should also be useful to determinate the optimal condition and procedures to produce nanostructures of interest as the pentagonal nanowires. These are few examples that indicate that our methodology will be intensively exploited in future studies for answering the interesting questions raised in the fascinating and useful domain of the nanowires.

9. Acknowledgment

We would like to thank A Hasmy, J J Sáenz, M Díaz, J L Costa-Krämer and E Medina for the interesting discussions and ideas. This work has been partially supported by the Spanish MICINN through Projects FIS2006-11170-C02-01 CSD2007-00046, and FIS2009-14320-C02 and by the Madrid Regional Government through the S-0505/MAT/0202 (NanoObjetos-CM) project. PG-M acknowledges the Spanish MEC "Ramón y Cajal" Programme support.

10. References

Agraït, N.; Levy Yeyati, A. & Van Ruitenbeek, J. M. (2003). *Physics Report*, 377, 81-279, ISSN: 0370-1573.

Bahn, S. R. & Jacobsen, K. W. (2001). *Phys. Rev. Lett.*, 87, 2661101, ISSN: 0031-9007.

Barnet, R. N. & Landman, U. (1997). *Nature*, 387, 788-791, ISSN: 0028-0836.

Branício, P. S. & Rino, J. P. (2000). *Phys. Rev. B*, 62, 16950-16955, ISSN: 1098-0121.

Bratkovsky, A. M.; Sutton, A. P. & Todorov, T. N. (1995). *Phys. Rev. B*, 52, 5036-5051, ISSN: 1098-0121.

Bulienkov, N. A. & Tytik, D. L. (2001). *Russ. Chem. Bull. Int. Ed.*, 50, 1-19, ISNN: 1066-5285.

Daw, M. S. & Baskes, M. I. (1983). *Phys. Rev. Lett.*, 50, 1285-1288, ISSN: 0031-9007.

Foiles, S. M. (1985). *Phys. Rev. B*, 32, 3409-3415, ISSN: 1098-0121.

García-Mochales, P.; Peláez, S.; Serena, P. A.; Medina, E. & Hasmy, A. (2005). *Appl. Phys. A*, 81, 1545-1549, ISSN: 0947-8396.

García-Mochales, P.; Paredes, R.; Peláez, S. & Serena, P. A. (2008a). *Nanotechnology*, 19, 225704, ISSN: 0957-4484.

García-Mochales, P.; Paredes, R.; Peláez, S. & Serena, P. A. (2008b). *Journal of Nanomaterials*, 2008, 361464, ISSN: 1687-4110.

García-Mochales, P.; Paredes, R.; Peláez, S. & Serena, P. A. (2008c). *Phys. Status Solidi A*, 205, 1317-1323, ISSN: 1862-6300.

González, J. C.; Rodrigues, V.; Bettini, J.; Rego, L. G. C.; Rocha, A. R.; Coura, P. Z.; Dantas, S. O.; Sato, F.; Galvao, D. S. & Ugarte, D. (2004). *Phys. Rev. Lett.,* 92, 126102, ISSN: 0031-9007.

Grigoryan, V. & Springborg, M. (2003). *Chem. Phys. Lett.*, 375, 219-226, ISSN: 0009-2614.

Gülseren, O.; Ercolessi, F. & Tosatti, E. (1998). *Phys. Rev. Lett.*, 80, 3775-3778, ISSN: 0031-9007.

Hasmy, A.; Medina, E. & Serena, P. A. (2001). *Phys. Rev. Lett.*, 86, 5574-5577, ISSN: 0031-9007.

Hasmy, A.; Pérez-Jiménez, A. J.; Palacios, J. J.; García-Mochales, P.; Costa-Krämer, J. L.; Díaz, M.; Medina, E. & Serena, P. A. (2005). *Phys. Rev. B*, 72, 245405, ISSN: 1098-0121.

Heemskerk, J. W. T.; Noat, Y.; Bakker, D. J.; Van Ruitenbeek, J. M.; Thijsse, B. J. & Klaver, P. (2003). *Phys. Rev. B*, 67, 115416, ISSN: 1098-0121.

Herrman, H. J. & Stanley, H. E. (1984a). *Phys. Rev. Lett.*, 53, 1121-1124, ISSN: 0031-9007.

Herrman, H. J. & Stanley, H. E. (1984b). *J. Phys. A: Math. Gen.,* 17, L261-266, ISSN: 1751-8113.

Ikeda, H.; Qi, Y.; Cagin, T.; Samwer, K.; Johnson, W. L. & Goddard III, W. A. (1999). *Phys. Rev. Lett.*, 82, 2900-2903, ISSN: 0031-9007.

Jacob, D.; Fernández-Rossier, J. & Palacios, J. J. (2005). *Phys. Rev. B*, 71, 220403, ISSN: 1098-0121.

Liang, W. & Zhou, M. (2006). *Phys. Rev. B*, 73, 115409, ISSN: 1098-0121.

Liang, W. & Zhou, M. (2007). *Philos. Mag.*, 87, 2191-2220, ISSN: 0141-8610.

Medina, E.; Díaz, M.; León, N.; Guerrero, C.; Hasmy, A.; Serena, P. A. & Krämer, J. L. (2003). *Phys. Rev. Lett.*, 91, 026802, ISSN: 0031-9007.

Mehrez, H. & Ciraci, S. (1997). *Phys. Rev. B*, 56, 12632-12642, ISSN: 1098-0121.

Mishin, Y.; Farkas, D.; Mehl, M. J. & Papaconstantopoulos, D. A. (1999). *Phys. Rev. B*, 59, 3393-3407, ISSN: 1098-0121.

Olesen, L.; Laegsgaard, E.; Stensgaard, I.; Besenbacher, F.; Schiøtz, J.; Stoltze, P.; Jacobsen, K. W. & Nørskov, J. K. (1994). *Phys. Rev. Lett.*, 72, 2251-2254, ISSN: 0031-9007.

Pauly, F.; Dreher, M.; Viljas, K. J.; Häfner, M.; Cuevas, J. C. & Nielaba, P. (2006). *Phys. Rev. B*, 74, 235106, ISSN: 1098-0121.

Peláez, S.; Guerrero, C.; Paredes, R.; Serena, P. A. & García-Mochales P. (2009). *Phys. Status Solidi C*, 6, 2133-2138, ISSN: 1610-1634.

Rapaport, D. C. (1995). *The Art of Molecular Dynamics Simulation*, Cambridge University Press, ISBN: 0521599423, Cambridge, United Kingdom.

Serena, P. A. & García, N. (Ed.) (1997). *Nanowires* (*NATO ASI Series E* vol 340), Kluwer Academic Publishers, ISBN: 0792346270, Dordrecht, The Netherlands

Sen, P.; Gülseren, O.; Yildirim, T.; Batra, I. P. & Ciraci, S. (2002). *Phys. Rev. B*, 65, 235433, ISSN: 1098-0121.

Sharvin, Y. V. (1965*). Sov. Phys. JEPT*, 21, 655-656, ISSN: 0038-5646.

Sirvent, C.; Rodrigo, J. G.; Vieira, S.; Jurczyszyn, L.; Mingo, N. & Flores, F. (1996). *Phys. Rev. B*, 53, 16086-16090, ISSN: 1098-0121.

Sørensen, M. R.; Brandbyge, M. & Jacobsen, K. W. (1998). *Phys. Rev. B*, 57, 3283-3294, ISSN: 1098-0121.

Sutrakar, V. K. & Mahapatra, D. R. (2009). *Nanotechnology*, 20, 045701, ISSN: 0957-4484.

Tsai, D. H. (1979). *J. Chem. Phys.*, 70, 1375-1382, ISSN: 0021-9606.

Electrodeposited Nanowires and their Applications

Edited by Nicoleta Lupu

ISBN 978-953-7619-88-6
Hard cover, 228 pages
Publisher InTech
Published online 01, February, 2010
Published in print edition February, 2010

The book offers a new and complex perspective on the fabrication and use of electrodeposited nanowires for the design of efficient and competitive applications. While not pretending to be comprehensive, the book is addressing not only to researchers specialized in this field, but also to Ph.D. students, postdocs and experienced technical professionals.

How to reference

In order to correctly reference this scholarly work, feel free to copy and paste the following:

Samuel Peláez, Carlo Guerrero, Ricardo Paredes, Pedro A. Serena, and Pedro García-Mochales (2010). Modelling Metallic Nanowires Breakage for Statistical Studies: Ni Case as Example, Electrodeposited Nanowires and their Applications, Nicoleta Lupu (Ed.), ISBN: 978-953-7619-88-6, InTech, Available from: http://www.intechopen.com/books/electrodeposited-nanowires-and-their-applications/modelling-metallic-nanowires-breakage-for-statistical-studies-ni-case-as-example

INTECH
open science | open minds

InTech Europe
University Campus STeP Ri
Slavka Krautzeka 83/A
51000 Rijeka, Croatia
Phone: +385 (51) 770 447
Fax: +385 (51) 686 166
www.intechopen.com

InTech China
Unit 405, Office Block, Hotel Equatorial Shanghai
No.65, Yan An Road (West), Shanghai, 200040, China
中国上海市延安西路65号上海国际贵都大饭店办公楼405单元
Phone: +86-21-62489820
Fax: +86-21-62489821